CHAPTER IV

Versatile Site-Selective Patch Patterning on Au Tetrahedra with Polymer Patches

The work in this chapter is part of a collaboration with Qian Chen's group at the University of Illinois at Urbana-Champaign and Thi Vo at the Johns Hopkins University. Our collaborators in the Chen group performed all the experimental work alluded to in the text and Thi performed all the theory calculations.

4.1 Introduction

Tetrahedral shapes and motifs are commonly seen in atomic and molecular systems, from the single molecule of methane (CH4) to the corner-sharing tetrahedra in magnetic pyrochlore lattices[98]. Tetrahedral particles as a class of unique shape have been extensively studied in colloids and nanoscience for their packing and assembly into quasicrystal[99, 43], 1D tetrahelix, 2D chiral lattices[100, 101], and other complex structures. Among those assemblies, tetrahedra mostly align their faces, sometimes with offsets, due to strong van der Waals or other interactions. Even entropic forces favor slightly offset face-to-face alignment of tetrahedra at intermediate densities[102]. To unlock more binding modes from tetrahedral particles, including the corner-sharing and edge-sharing modes naturally existing in atomic systems, additional directional bonds are required from regioselective surface coding

or patterning. Nanoparticles (NPs) decorated with controlled shape, size, and discrete numbers of chemical or topological patches on their surface, known as patchy NPs[103], are promising candidates in introducing directional and specific bonding to the NP assembly systems. The dual structural and chemical heterogeneity make patchy NPs intriguing for fundamental studies in colloids, fabrication of complex and programmable nanostructures, and exploiting far-reaching applications in sensing[104], catalysis[105], and biomedicine[106].

During the past decade, increasing efforts have been contributed to generating polymeric patches on the surface of metallic NPs with controlled patch size, shape, number, and positioning. Multiple strategies have been reported for site-selective patch growth including polymer segregation in selective solvent[107], wetting-induced phase separation of mixed ligands[108], and curvature-preferred ligand grafting[96]. These methods have shown success on isotropic NPs or simpler anisotropic shapes, like rods and cubes, in generating one or two typical structures of patches on each shape. To date, we have seen no methods applied to a complex shape like the tetrahedron to generate various types of patches with high regioselectivity or precise control over patch number, size, and shape.

Here we design a versatile model system of patchy tetrahedra composed of NP cores of gold tetrahedra (94 nm) and polymeric patches of polystyrene-b-polyacrylic acid (PS-b-PAA, 16k-b-3.7k) with controlled positions and patterns: vertex patched, edge patched, clover-like, vertex and edge patched, and face patched tetrahedra. By tailoring the adsorption of surface ligands on the Au tetrahedral cores and the solvent quality for the PS-b-PAA chains, we can control the size, shape, number, and positioning of the surface patches with high precision. Representative patchy tetrahedron structures, as well as the patch size and shape, are demonstrated with

agreement between experiment and molecular dynamics (MD) simulation. Patch dimension and positioning on Au tetrahedra is prescribed by the stenciled patterning of two competing molecules: the masking molecule, iodine (I-), prohibits the adsorption of polymer chains onto (111) facets, whereas the anchoring molecule, 2-naphthalenethiol (2-NAT), facilitates the grafting of polymers to form patches on the unmasked surface of Au tetrahedra.

We study patch pattern trends in a phase space of different iodine and 2-NAT concentrations, mimicking the same trends with corresponding simulation variables and demonstrate agreement between simulation and experiments. We further study the effect of solvent quality and tetrahedra size (69nm) in simulation by comparison of the corresponding patch diagrams.

4.2 Synthesis of Patchy Tetrahedra with Iodine Masking

The Au tetrahedra were first synthesized and purified by the Chen group using the method reported in previous work[101]. Stock solutions of Au tetrahedra were prepared in 20 mM CTAC and incubated with sodium iodide (NaI), as the iodine atoms are known to preferably bind to the (111) facets of Au, at controlled concentrations. Next, aqueous suspensions of iodine-masked tetrahedra at fixed concentration were mixed with 2-naphthalenethiol (2-NAT) and PS-b-PAA in the mixture of dimethyl formamide (DMF) and water in a one-pot procedure at 110℃ to induce polymer patch formation. The PS blocks of the polymers can adsorb onto the 2-NAT covered area via hydrophobic attractions and the PAA blocks develop a brush conformation in the good solvent. The solvent mediates the chain-chain interactions and induce the collapsing of the polymer brushes when the solvent quality decreases (by increasing the water content). The representative structures produced through the Chen

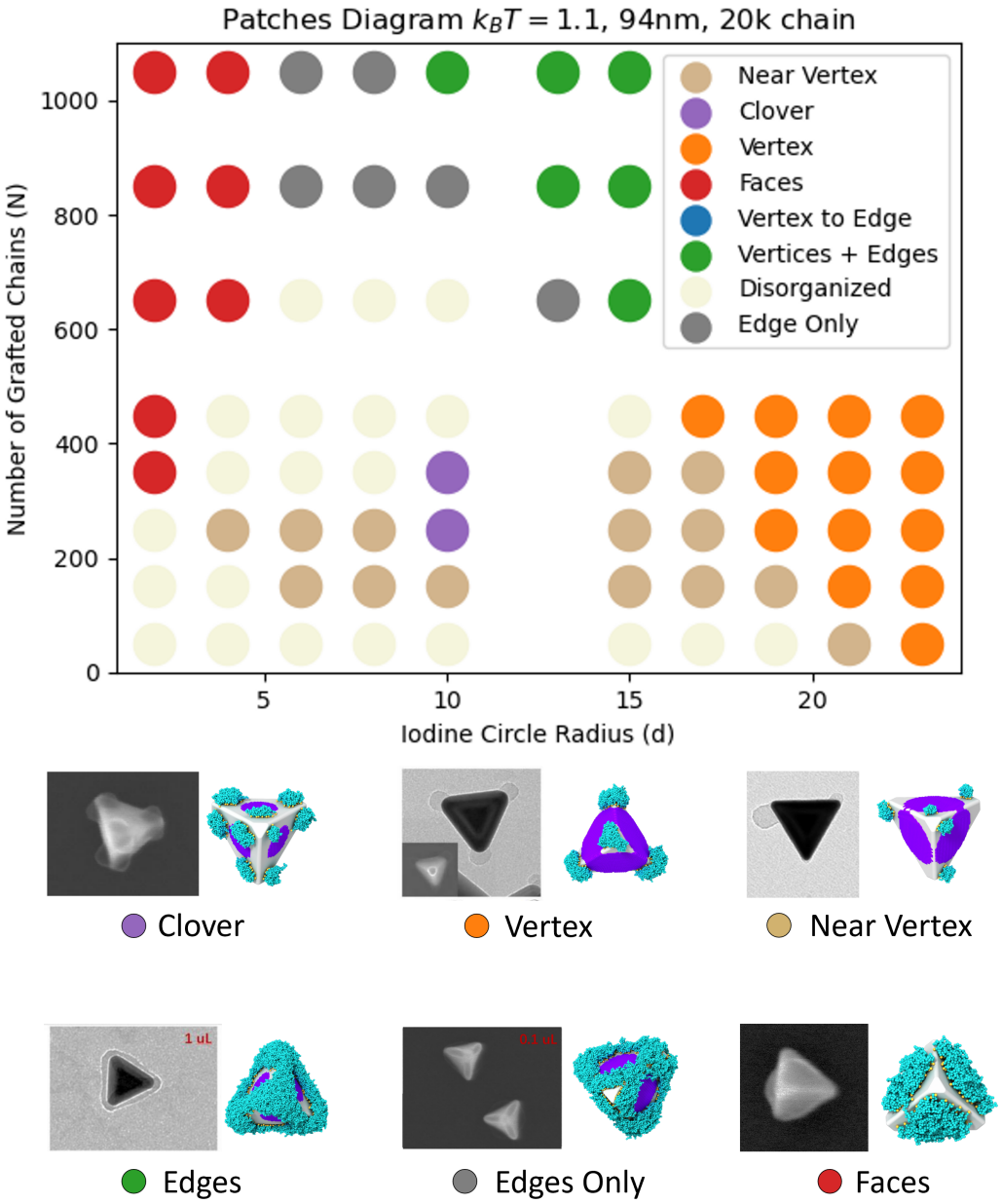

Figure 4.1: Synthesis and simulation of iodine-masked tetrahedra. Top: phase diagram across a range of iodine circle radii d and number of grafted polymers N. We use simulation parameters corresponding to the model system of 94nm tetrahedron with 20k chain and temperature corresponding to lower experimental water content. Bottom: Comparison of patch patternings between simulation and experiment for each phase observed.

group's methods show great definition in the SEM images at the bottom of Fig. 4.1.

Correspondingly, we simulate the model system using the procedure described in

Section 4.5. Briefly, we simulate a single tip-truncated tetrahedron with a surface region covered by poison particles, modeling the iodine region of the core surface centered on the large (111) faces and extending outward in a circle of radius d. We place N polymer chains with 20 monomers to model the PS-b-PAA polymer. We use d as a proxy for iodine concentration in simulation and N as a proxy for 2-NAT concentration. We run simulations at many combinations of N and d and obtain the patch diagram shown in Fig. 4.1. We find all patch patterns found in experiment, with comparisons shown at the bottom of Fig. 4.1.

By inspection of the phase diagram, we see important trends in both the low N and high N limits. At low N and small d, much of the surface is unmasked and small patches choose to sit near the vertex of the tetrahedron due to the entropic favorability provided[86]. If the conditions are just right, a patch will sit on each of the 12 near-vertex regions forming the "clover" phase. As d increases at low N, the iodine covers more and more of the (111) facets and forces the polymer chains to the tip of the particle, forming the "vertex" phase.

At high N and small d, the polymers form larger patches that cover the entire surface of the large faces to minimize potential energy. As we increase d at high N, the iodine pushes the polymer chains off the faces of the tetrahedron, forcing them to the edge and near-vertex regions, rather than the small truncated vertices, forming the "edge-only" phase. We believe the patches avoid the small vertex truncated regions whenever possible to minimize the chain stretching energy penalty associated with patches spreading across multiple faces. In this system, the tip truncation is small, so patches cannot fit entirely on the truncated tip facet. At high N and high d, however, the polymers are once again pushed to the vertices and edges of the shape, forming the "edges" phase.

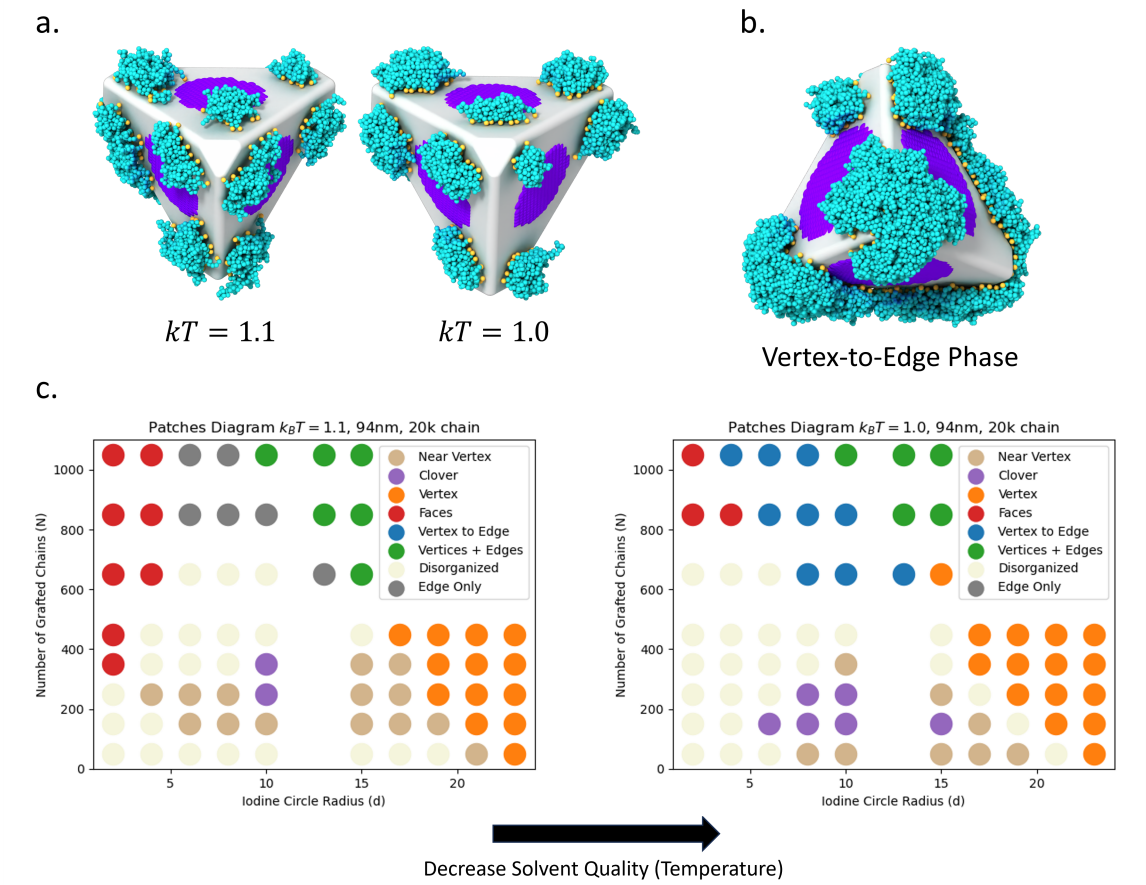

Figure 4.2: Effect of changing solvent quality. Decreasing the solvent quality increases patch clarity (a). It shrinks the face patched region and increases the clover patched regions of the phase diagram (c). It also introduces a metastable state replacing the edge region from the higher temperature, which we label vertex-to-edge in the phase diagram (b, c).

4.3 The Effect of Solvent Quality

We now investigate the effect of changing the solvent quality on the phase diagram. Decreasing the solvent quality is achieved experimentally by adding more water to the solvent, augmenting the hydrophobic attraction of the PS blocks on the polymer chains and increasing the interaction strength. We model increases in interaction strength in our simulations by lowering the simulation temperature. Qualitatively, lowering the solvent quality sharpens the patch definition (see Fig. 4.2a)

and prioritizes monomer-monomer interactions rather than the entropic freedom of the chains. This has three effects on the patch diagram in Fig. 4.1: reducing the size of the "faces" region, increasing the size of the "clover" region, and introducing a metastable phase in the region previously occupied by the "edge-only" phase.

The reduction in the size of the "faces" region occurs due to the reduction in patch volume, needing more chains to occupy the entire (111) face of the shape. This trend can be seen in Fig. 4.2c where the region of the phase diagram at lower N changes from the "faces" phase to "disorganized". The size of the "clover" region in the phase diagram increases because monomer-monomer interactions are prioritized and the energy cost of chain stretching over the facet boundary is increased, therefore encouraging patches to remain separate. Additionally, the lower temperature (higher interaction energy) appears to create a metastable phase, which we call "vertex-to-edge", in the phase diagram. The "vertex-to-edge" phase is shown in Fig. 4.2b and is defined by a subset of the shape's vertices and edges being covered in a way that breaks the shape's symmetry. We anticipate that thermal annealing performed in this region of the patch diagram would remove this phase from the phase diagram.

4.4 The Effect of Particle Size

To model the effect of changing particle size, we run a set of simulations at a core radius of $R_0 = 8.49$ instead of the previous value of $R_0 = 11.57$. Decreasing the core size while keeping the chain length fixed has the equivalent effect of increasing the polymer chain length, as polymer chain behavior is determined by the ratio of the polymer radius of gyration to the size of the core R_g/R_0.

As shown in Fig. 4.3, the primary effect of increasing chain length (decreasing core size) is the disappearance of the "clover" phase. Rather than remain in separate small

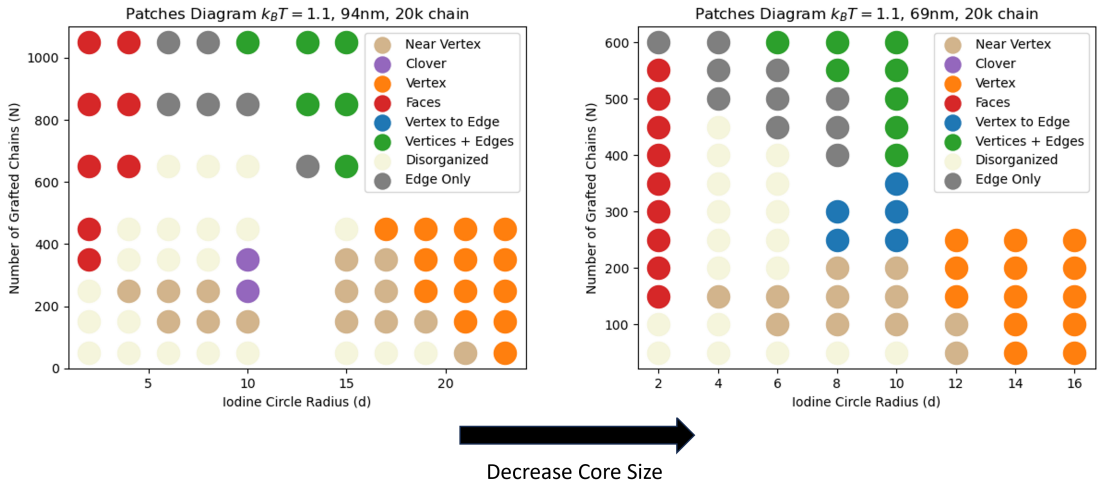

Figure 4.3: The effect of changing particle size. The biggest trend in making the particle size smaller is the disappearance of the clover phase, due to the chains ability to stretch across the facets that separate the patches in the clover phase. The appearance of the vertex-to-edge phase is an artifact of our classification algorithm rather than a signficant trend in patch patterning.

patches, longer chains in the "near-vertex" regions bridge together to minimize their energy and form a ring around the tetrahedron vertex. We also note that in the phase diagram of Fig. 4.3, the "vertex-to-edge" region appears in the phase diagram for the smaller particle. We consider this to be an artifact of our classification criteria, which we explain further in Section 4.5.2, rather than a significant behavioral trend.

4.5 Methods

4.5.1 Molecular Dynamics

We run molecular dynamics (MD) simulations of truncated tetrahedra grafted with N polymer chains with two different insphere radii $R_0 = 8.49, 11.57$. We statically place a dense region of poison particles centered at each large face defined by a circle of radius d to restrict the surface area available to the polymer chains, similar to Chapter III. To model our polymers, we use bead-spring chains with 20 monomers, FENEWCA bonds, and the anisotropic Lennard-Jones potential[83] for nonbonded

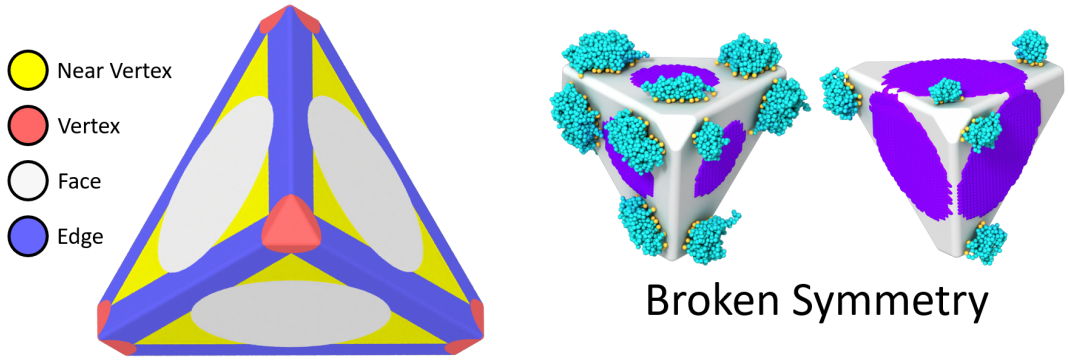

Figure 4.4: Method of classifying patch patterns. (Left) We partition the surface of the core into 4 regions, compute the monomer density in each region, and classify the pattern based on which regions have high density. (Right) In some cases, this method fails when two phases are the same up to a broken symmetry like the clover and near-vertex patterns.

interactions, similar to Chapter III. We do not explicitly model the non-poison particles covering the surface as was done in Chapter III because we determined that they did not impact simulation results to any significant degree.

Our MD simulations were run in HOOMD-Blue[79] in the NVT ensemble with $kT = 1.0$ and 1.1 for simulations modeling solvent with higher and lower water concentration, respectively. We first run our simulations for 10^6 timesteps using $dt = 10^{-4}$ with WCA polymer-polymer interactions to let the polymer explore the surface of the core. After that, we set the polymer-polymer attractions to be attractive Lennard-Jones and run the simulation for between 1×10^7 and 2×10^7 timesteps to allow for proper equilibration depending on the number of grafted polymers N.

4.5.2 Classifying Patch Patterns

We classify patch patterns by computing the local monomer density in four relevant regions of the core surface: *face*, *vertex*, *edge*, and *near-vertex*. We define each region mathematically via a series of dot and cross product operations on the position of each monomer, resulting in a partition shown visually on the left of Fig. 4.4. In each simulation frame we compute the local density of the monomers in each region

and average over the frames. Each simulation is then classified based on the shape regions that are high density. For example, the "clover" pattern has high density in the *near-vertex* region and nowhere else. The "edge-only" pattern has high density in the *edge* and *near-vertex* regions and low density in the *face* and *vertex* regions.

This algorithm works well except in cases where two patterns are the same up to a broken symmetry or where no region has significantly higher density than any other. In such cases we have to use other classification methods, or our best judgement. For example, the "clover" and "near-vertex" patterns have high density in the same region (*near-vertex*), but they are different because of a broken symmetry (Fig. 4.4, right). In this case, we differentiate the two patterns by establishing a cutoff number of patches on the core surface. To be considered the "clover" pattern, the particle has to have 9 or more patches on the core surface. In cases where there is a similar monomer density in each region, we have to decide between the" disorganized" and "vertex-to-edge" pattern. In this case we count the number of covered vertices and edges. If the number of covered vertices is between 1-3 and the number of covered edges is between 2-5, we consider it the "vertex-to-edge" pattern.

4.6 Conclusions

In this work, we modeled of a variety of experimental tactics for the synthesis of patchy polymer-grafted nanoparticles for greater control over the resulting patch patterns. We first explained our simulation model, including how we map simulation variables to their experimental counterparts. We then demonstrated the effects of changing both iodine and 2-NAT concentration, showcasing "faces", "edge", "edges-only", "near vertex", "clover", and "vertex" patterns in different regions of the phase diagram. We then extended the range of experimental variables we modeled in

simulation by generating similar patch diagrams to model changes in solvent quality and particle size. Changing the solvent quality has the effect of changing the size of the regions occupied by various patterns in the phase diagram, and changing the particle size has the effect of removing the "clover" phase from the patches diagram. This work provides a path forward for the synthesis of particles that can assemble into crystal structures that may arise from corner and edge sharing tetrahedral motifs, as well as the potential for chiral motifs arising from selective patch bonding of the "clover" pattern.

CHAPTER V

Computational Tools for Nanoparticle Self-Assembly

5.1 Introduction

Computational tools provide researchers with the ability to conduct science in time scales which are orders of magnitude smaller than experiment. From modeling and simulation of systems of interest, to visualizing large-scale data pipelines, to solving and visualizing solutions to equations that cannot be solved analytically, computation has enhanced our ability to conduct science at every stage of the research process.

In the world of NP self-assembly, simulation is critically important for understanding how NP building blocks self-assemble into bulk crystal structures exhibiting long range order. Much effort has been put into leveraging modern computing devices like GPUs to simulate systems of up to millions of particles as fast as possible. A typical experiment may take months to complete, but a simulation of the same system may now take only a few hours with advanced computing hardware. To prevent the research bottleneck from shifting to the analysis side of the workflow, tools that analyze the simulation's output data are also being designed to complete the needed analyses on a similarly fast time scale. The rate at which research can be done in soft matter depends on the quality of the computational tools developed to achieve the research goals.

One problem of particular interest in the world of soft matter self-assembly is the ability to quickly and efficiently determine which NP building blocks yield desired self-assembled crystal structures. There are essentially two solutions to the problem: high-throughput screening and inverse design. High-throughput screening leverages a fast calculation of the forward problem (what structure will my building blocks assemble?) to find the desired crystal structure in the large phase space of possible building block combinations. The inverse problem (what building blocks will give me the structure I want?) is a much more direct route to getting the desired crystal structure, however, it is much more complicated to solve due to the nature of the optimization problem involved. Solving the inverse problem is considered a "holy grail" in our field, essentially removing all doubt in choosing the needed building blocks to creating novel materials. In the subsequent sections I will discuss my software contributions that aid in solving the above problems in computational soft matter.

5.2 Extended Digital Alchemy

5.2.1 Background

HOOMD-blue[109] is a particle simulation engine first developed in 2008, originally geared towards large-scale GPU MD simulations[110]. Since then, it has grown into a toolkit for other simulation algorithms, most notably including HPMC[111]. To satisfy science's ever-growing need for a wide variety of simulation methods and protocols, we re-designed its interface during my Ph.D. years between 2019 and 2021, culminating in the version 3.0.0 release. The re-designed API introduced an object-oriented, modular design with a wider variety of customization options including most notably custom actions, forces, and log quantities. Custom actions and forces are pure python classes written by users that plug into simulations similarly

to HOOMD-blue's native classes. Custom log quantities allow users to log any simulation quantity they can compute in python to their choice of logging backend like GSD or HDF5. My contribution to the re-design included creating device objects, porting many components from the `md` module, and creating an API for users to create custom forces in python. The version 3 API also publicly incorporated recently developed simulation methods like the Anisotropic Lennard-Jones potential[83] and digital alchemy[112].

Digital alchemy is a computational method for inverse design by which we simulate an extended thermodynamic ensemble including additional degrees of freedom, called alchemical degrees of freedom, and their corresponding conjugate variables, called alchemical potentials. By running simulations in the extended ensemble, the system is allowed to find its free energy minimum, which should correspond to an optimized configuration of the alchemical degrees of freedom. In the past, this method has been applied to systems where either the particle shape[112] or patch interactions[113] are individually optimized. However, to obtain the holy grail of inverse design, we need a tool that can additionally optimize patch locations and/or optimize all three variables (shape, interactions, locations) concurrently across any functional form of patch interaction, strength, and range. To this end, I developed a set of custom plugins to HOOMD-blue implementing a software framework to extend the range of systems we can design with digital alchemy.

5.2.2 Patch Location Move Algorithm

One additional alchemical degree of freedom we need to simulate is the location of patch interaction sites on the surface of a particle's shape. We therefore must devise a scheme for proposing Monte Carlo moves on the surface of shaped particles. We propose the following algorithm for proposing trial moves, which we call the patch

move algorithm and illustrate in Fig. 5.1a and Fig. 5.1b:

1. Compute the unit vector n_i for each patch location p_i on the particle surface.
2. Propose a uniform random move in orientation (θ, ϕ) space for each unit vector n_i, resulting in unit vector n_i'
3. Project n_i' onto the particle surface to get the trial move location p_i'

This patch move algorithm has several desirable features. First, it both obeys detailed balance and is ergodic for all convex shapes. This is because there is a 1-1 mapping between unit vectors and points on the particle surface for convex shapes. A more generic move algorithm for concave shapes might require making moves on the shape's polyhedral net with periodic boundary conditions, but this is more complex to implement. Second, the patch move algorithm can be computed quickly. Making a random orientation move is algorithmically simple[114] and projecting the unit vectors to the surface of the shape amounts simply to solving the ray-plane intersection problem for each face of the shape. While the patch move algorithm is ergodic, it does not sample each location on the surface of the shape with equal probability. For example, elongated shapes will sample higher curvature regions of the surface less frequently than lower curvature regions. For this reason, simulating highly elongated shapes may require either longer simulations or a different patch move algorithm.

5.2.3 Implementation

We implement patch location and patch interaction moves as custom updaters in HOOMD-blue. In the interest of modularity, we propose particle shape, patch interaction, and patch location moves separately so any subset can be used in a digital alchemy simulation in any combination. Additionally, we provide custom python

classes for logging patch locations and additional utilities for proper visualization and analysis of systems with mobile patch locations.

Patch location moves are implemented using the standard Monte Carlo metropolis criterion in a custom python updater, where a single proposed move changes the location of all patches on the particle shape surface. We use a separate class corresponding to the HPMC integrator in HOOMD-blue to implement the patch move algorithm described in the previous section.

Due to the wide variety of patch interaction potentials, optimization schemes, and constraints on the patch interaction parameters, patch interaction moves are implemented by allowing the user to define their own class and implement the `propose_parameter_moves` method, which takes a set of random move sizes and a dictionary of the current patch interaction parameters and returns a dictionary of proposed new parameters. The custom user class is used by another custom action, which calls the `propose_parameter_moves` method and then uses the standard Metropolis criterion to accept or reject the proposed patch interaction move.

HOOMD-blue does not write patch position or diameter data to GSD files by default, so we provide a utility function and a set of custom log quantities for easy conversion and visualization of simulation data. Users are expected to log patch positions and diameters to GSD files using the plugin's provided custom log quantities, which they then give to a conversion function after the simulation finishes running. The conversion function takes the logged patch locations and diameters and writes a new GSD file with the logged data written as particle data.

5.2.4 Results

We test the patch move algorithm's ability to find the free energy minimum of a system of patches on hard particles by fixing truncated tetrahedra in the positions

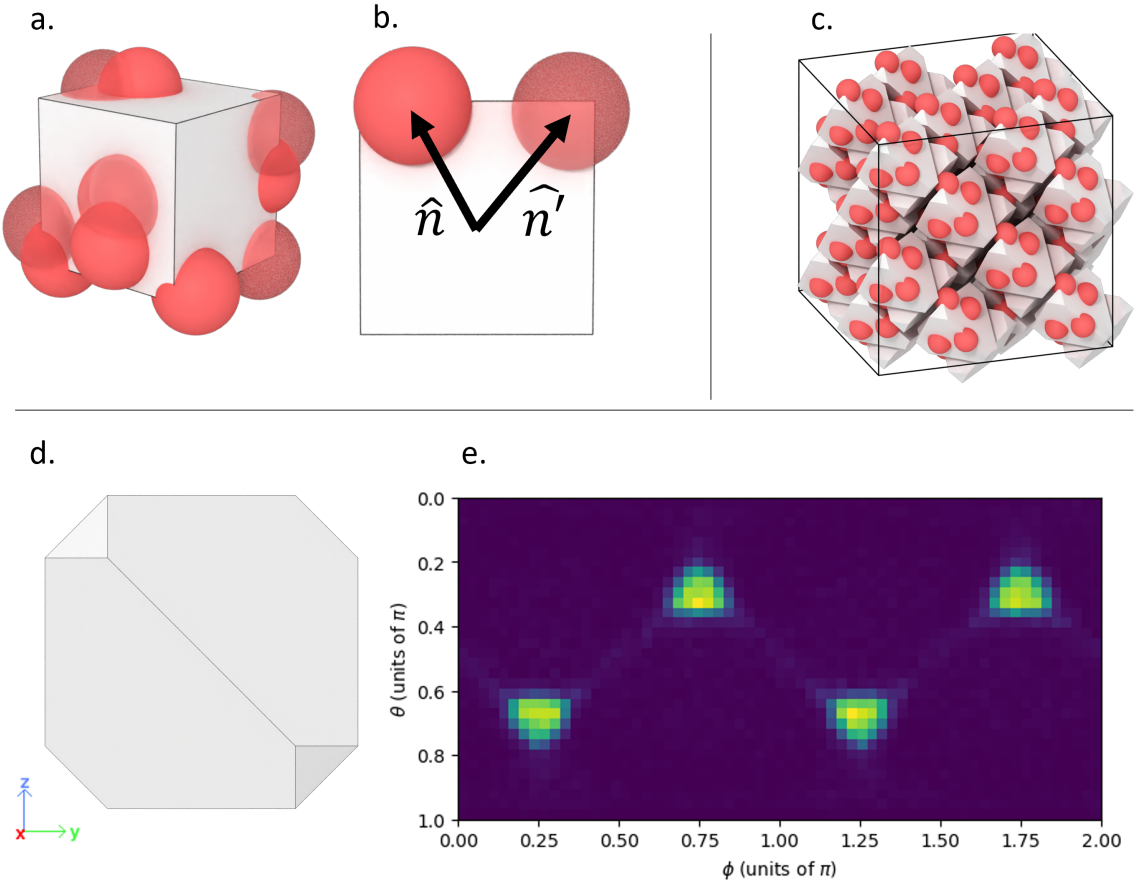

Figure 5.1: Patch location moves on convex polyehedra. The patch move algorithm (a,b) defines a unit vector $\hat{n}$ to each patch, makes a random move in orientation space resulting in $\hat{n}'$ and projects $\hat{n}'$ to the surface. A single move is proposed for all patches at once. We then study a system of truncated tetrahedra with four patches in cubic diamond (c). The lowest energy configuration of the system is with corner patches, and the orientational heatmap (d,e) demonstrates the system finds and stays at this lowest energy configuration for much of the simulation.

and orientations of a perfect cubic diamond lattice of 64 particles. As shown in Fig. 5.1c, we initially place four patches in random locations on the particle surface interacting via a square well potential with the interaction strength $\epsilon = 3.0$ and interaction width $\sigma = 1.0$ on each tetrahedron. We then run HPMC simulations in HOOMD-blue with custom patch location updater implementing the patch move algorithm for 10^7 MC sweeps to ensure plenty of statistics. We then compute the orientational heatmap (Fig. 5.1d and Fig. 5.1e), demonstrating the patches spend much of the simulation time in the lowest energy configuration while simultaneously remaining ergodic.

5.2.5 Future Work

Continuing work will first need to focus on extending the particle shape move algorithm already implemented in HOOMD-blue to shapes with patches on the surface. Specifically, particle shape move must ensure patches remain on the shape to prevent invalid system configurations intra-timestep. Additionally, the patch energy change induced by the particle shape move must be accounted for in the shape move's Metropolis criterion. We anticipate these details can be incorporated with minor revisions to the current particle shape move algorithm in HOOMD-blue.

Most of the future effort will be focused on devising more intelligent trial move algorithms that can help the system minimize its free energy more effectively. The algorithms we have added thus far have been straightforward Monte Carlo importance sampling, which likely won't suffice as more alchemical degrees of freedom are utilized in simulation because non-convex optimization over an increasingly large alchemical parameter space makes finding a global minimum increasingly difficult. In the interest of modularity, our algorithms treat proposed patch location, particle shape, or patch interaction moves separately, while a more complex global optimization al-

gorithm might propose them together to help better guide the extended ensemble towards a free energy minimum.

5.3 Agrippa

5.3.1 Background

Polymers are an essential nanoscale building block for the design of NP crystal structures due to their ability to influence NP bonding behavior. An understanding of polymer behavior on the surface of shaped NPs is therefore essential for understanding NP self-assembly. Previous work[86, 75, 115] has demonstrated the usefulness of a scaling theory for prediction of polymer behavior on shaped NPs in the intermediate length regime. Combined with a lattice perturbation theory[116], the scaling theory has been shown to be useful for end-to-end prediction of the lowest potential energy of a set of candidate crystal structures knowing only the NP building blocks which are used in experiment. The method has been used in isolated cases, yet it is both useful for high-throughput screening and is generalizable to a wide variety of NP systems, so it fits the criteria for the lazy refactoring approach to scientific software[117]. We therefore present *agrippa*, a package for the prediction of polymer-grafted NP effective shapes and the corresponding lattice energies of these effective shapes arranged into periodic colloidal crystal structures.

5.3.2 Effective Shape Calculations

The first core feature of *agrippa* is the calculation of nanoparticle effective shapes like those predicted and used in the previous chapters of this thesis. The most fundamental object in agrippa is the `Nanoparticle`, which is decomposed further into a `Core` and a `Corona`. Both the `Core` and the `Corona` have a set of points defining their surface, however the `Core` also encapsulates the core shape and exposes the associated

geometric properties. The points defining the graft sites on the core surface can be selected via either a random algorithm in which graft sites are selected in a uniform random distribution, or an ordered algorithm preserves consistent spacing between graft sites.

Once a core shape and method of placing graft sites is selected, polymer chains can be grafted to the core using the `graft` module. There are two graft algorithms: the `MC` algorithm and the `FloryMC` algorithm. The `MC` algorithm selects a set of graft sites on the core weighted by the free energy of a polymer attaching to that location on the core surface. The free energy is given by [86]

$$F(\Omega) = \frac{(R_{chain} - r_0)^2}{Nb^2} + \frac{\nu\sigma r_0^2 N^2}{(\Omega R_{chain})^3}, \tag{5.1}$$

where r_0 is the core insphere radius, N is the degree of polymerization of the polymer chain, b is the Kuhn segment length of the chain, ν is the monomer excluded volume, σ is the grafting density, Ω is the core curvature parameter, and R_{chain} is defined by [86]

$$R_{chain} \sim r_0 \sigma^{1/5} \nu^{1/5} b^{2/5} \left(\frac{Nb}{\Omega r_0}\right)^{3/5}. \tag{5.2}$$

The `MC` algorithm repeats this procedure many times to obtain a graft probability p_{graft}, and then multiplies p_{graft} by Eq. 5.2, which defines the outer surface of the effective shape. This `MC` algorithm is appropriate when polymer chains either have a high grafting density, or interactions between polymer chains can be neglected. The more complex case is handled by the `FloryMC` algorithm.

In the `FloryMC` algorithm, the probability that a polymer attaches to a given graft site is modified by the presence of other polymers nearby. To accomplish this, all grafting sites that are within $R_g = R_{chain} - r_0$ of an attached chain are flagged so that chains that attach there have their excluded volume modified by the Flory χ

parameter such that $\nu = b^3(1-2\chi)$[96]. The `FloryMC` algorithm should be used when the polymer chains have significant attraction to each other relative to other energy scales in the system. The `FloryMC` algorithm is the same as the `MC` algorithm in the limiting case of $\chi = 0$ (corresponding to infinite temperature), but the `MC` algorithm is much faster, so we recommend using `MC` whenever possible.

The chosen graft algorithm will populate the points on the outer extent of the nanoparticle corona defining the effective shape. Once the effective shape is defined, *agrippa* can compute lattice free energies of formation of colloidal crystals comprised of these shapes, and find the lowest energy among a set of target lattices.

5.3.3 Lattice Energy Calculations

The lattice energy calculations first require defining a set of potentials of mean force (PMFs) describing the interactions between the neighboring NPs. These PMFs must consider distance and relative orientation between neighbors. We do not *a priori* know the relative orientation of the effective shapes corresponding to the lowest lattice energy configuration. However, in most cases we can physically intuit from symmetry a few relative orientations likely corresponding to minima in the free energy landscape. To compute a PMF, we assume a relative orientation between effective shapes and a potential energy of interaction between points on the effective shape. We then compute the average energy between all pairs of points on the two effective shapes at a set of distances between particles using classes in the `pmf` module.

Once a PMF is defined at each relative orientation, the thermodynamic perturbation theory from [116] can be solved using the lattice energy module for a variety of target structures. To compute the relative free energy of formation dG for these lattices, we solve the following set of equations for dG given a single PMF $U(r)$ and

the pair correlation function for the target crystal $g_{crys}(r)$:

$$dG = -RT\log(K_{eq}), \tag{5.3}$$

$$K_{eq} = \frac{1}{\phi(m,n)!}\int f_M^{\phi(m,n)}(r)g_{crys}(r)dr, \tag{5.4}$$

$$f_M(r) = e^{-\beta U(r)} - 1, \tag{5.5}$$

$$\phi(m,n) = min(m,n). \tag{5.6}$$

After solving for dG for many target crystal structures and relative effective shape orientations (i.e. many PMFs), one can compare among many final lattice energies and find the optimal candidate (i.e. the crystal structure with the lowest lattice energy).

This completes the end-to-end workflow in which a preferred crystal structure can be identified from a set of candidates knowing only the parameters of the input nanoparticle core, ligand, and ligand interactions.

5.4 Shadow Projection Overlap of Obstacles for Neighbor Exclusion (SPOONE)

The work in this section was performed in collaboration with Dom Fijan, Charlotte Zhao, and Philipp Schönhöfer. All members provided intellectual contributions, helped implement the unweighted version of SPOONE, and analyzed SPOONE neighbors for the systems studied. The SPOONE concept was created by Dom, Philipp, and Charlotte. My contributions include designing the filter concept in *freud*, implementing the weighted version of SPOONE, and the ray density analysis.

5.4.1 Background

The *freud* library is a high-performance, particle trajectory analysis toolkit[80] intended to complement packages that implement molecular simulations. The *freud* library computes canonical simulation analyses such as RDFs and MSDs, order param-

eters such as Steinhardt[97], cubatic[118], solid-liquid[119], and hexatic[40], and a few more specialized analyses such as PMFTs[55, 120] and environment matching[121]. Many of the above analyses require defining particle neighborhoods as a precursor to performing the analysis.

The *freud* library implements a wide range of neighbor finding algorithms such as r_{max}, k-nearest, and Voronoi neighbors. Even with a physically relevant choice of parameters, the r_{max} and k-nearest algorithms may unphysically define particle neighborhoods such that neighbor particles may have other particles blocking them. Other neighbor definitions such as Relative Angular Distance (RAD)[122] and Solid Angle Nearest Neighbors (SANN)[123] were previously defined such that blocked particles cannot be considered neighbors. The RAD and SANN methods achieved their desired purpose for spherical particles, but they may provide non-intuitive neighbor definitions in systems of non-spherical or elongated particles. We therefore propose a new neighbor finding algorithm for shaped particles called the Shadow Projection Overlap of Obstacles for Neighbor Exclusion (SPOONE) algorithm.

5.4.2 Neighbor Definition

The SPOONE method defines a particle k to be a neighbor of a particle i if the shadow of particle i can be cast along the vector $\vec{r}_{ik}$ without the shadow overlapping any other particles j before reaching particle k (Fig. 5.2a). Because SPOONE defines its neighbors via the shadow cast from the surface of i towards k, the neighbor definition is in general asymmetric. There are two modes of defining how the shadow from i is cast towards k: parallel transport and screen. The first mode is called parallel transport, in which the shadow is projected from the surface of particle i only a distance equal to the neighbor distance r_{ik} before cutting off the shadow projection. The second mode is called screen, in which the shadow is projected onto

a screen centered at the origin of particle k, normal to the vector $\vec{r}_{ik}$ between the two particles. Functionally, the difference between the two modes is how far the shadow is projected along the neighbor vector $\vec{r}_{ik}$ before we no longer consider other particles j to be blockers.

5.4.3 Implementation

SPOONE is implemented in *freud* using ray tracing algorithms from Intel's embree[124] library. To shoot rays from particle i to particle k, a set of points on the surface of particle i, called the ray origins, must first be defined. The ray origins are computed by shooting rays of a user-supplied density, called the ray density ρ_{ray}, from the screen on particle k back towards particle i. The location where this set of rays intersect the surface of particle i are the ray origins. A second set of rays are then shot from the ray origins towards particle k a distance defined by the mode (parallel transport or screen, see previous section). If any ray shot from a ray origin hits a particle other than k, particle k is considered blocked and is not a neighbor of particle i.

In the interest of performance, we use a multithreaded model where each worker thread finds the neighbors of a given particle i and thread-local neighbor lists are merged at the end of the implementation. For large systems and/or high ray densities, the performance of computing the SPOONE neighbor list may still be less than desired even with a parallel threading approach. In such cases, we recommend SPOONE be used as a method of removing blocked neighbors from a previously computed neighbor definition found via more performant methods like r_{max}.

5.4.4 Weighted Version

The SPOONE method has both weighted and unweighted versions. In the unweighted version, particle k is only a neighbor of particle i if there are no rays shot from the surface of particle i that hit another particle j. In the weighted version, any particle k for which a single ray shot from particle i makes contact is a neighbor with weight equal to the fraction of rays shot from particle i that do not hit a blocking particle j. The weight associated with each neighbor in the weighted version is therefore between 0 and 1.

The weighted definition of SPOONE results in a much larger set of neighbors than the unweighted version, most of which have small weights. We therefore propose a third way of defining neighbors with SPOONE, in which we compute the weighted SPOONE neighbors and afterwards remove any neighbors with weight less than a cutoff value w_{cut}. This method may be useful by providing more neighbors than the unweighted version, yet not include those neighbors that have very small shadow overlaps.

5.4.5 Comparison with other Neighbor Finding Algorithms

We now compare the SPOONE neighbor definition to that of other common neighbor-finding algorithms for a system of bipyramids with aspect ratio 3 exhibiting nematic order at a volume fraction $\phi = 0.54$ (Fig. 5.2b). In Fig. 5.2c, we show the number of neighbors for SPOONE weighted, SPOONE unweighted, r_{max}, RAD_{open}, RAD_{closed}, and SANN. The unweighted version of SPOONE has significantly fewer neighbors than all other neighbor definitions, which is expected given the definition only defines particles as neighbors if *all* rays shot from one particle hit another. The weighted version of SPOONE, in which we define the number of neighbors as the

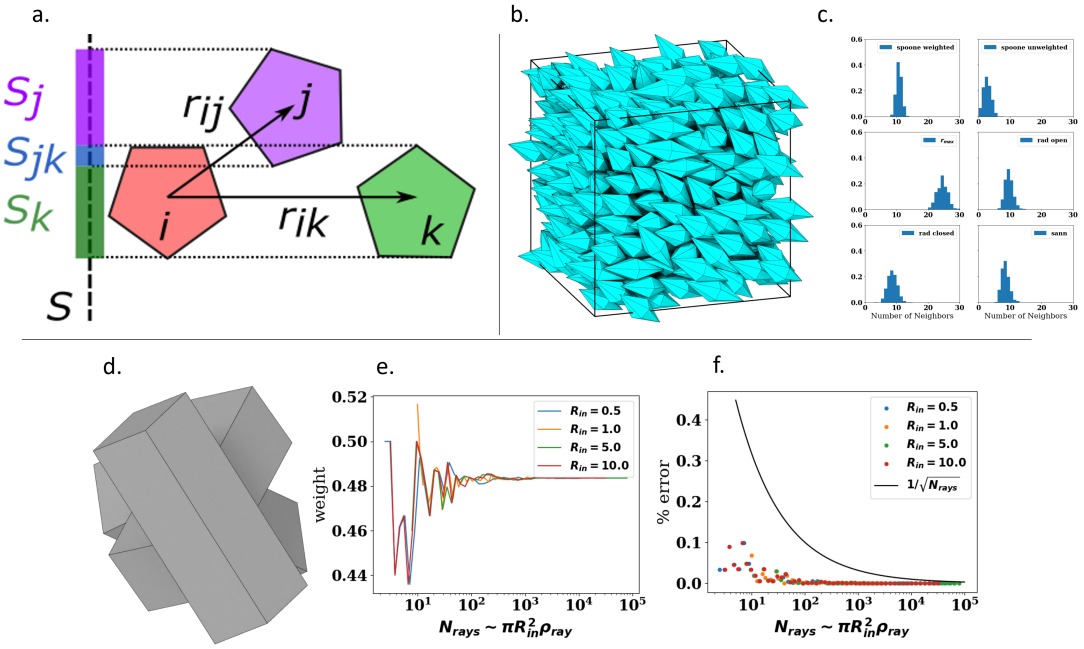

Figure 5.2: The SPOONE neighbor finding algorithm. (a) A visual depiction of the algorithm, in which two particles are only considered neighbors if the shadow projected along the neighbor vector, $\vec{r}_{ik}$ doesn't overlap with any other particles j. (b) Snapshot of bipyramids in the nematic phase. (c) Comparison of neighbor counts of many different neighbor finding algorithms on the shapshot from (b). (d) System of 3 square prisms along a line at random orientations. (e) SPOONE weight between two outermost particles in snapshot (d) as a function of ray density. (f) Plot of the error in the weight compared to the limiting value ($\rho_{ray} \to \infty$).

sum of weights across all weighted neighbors, is generally consistent with other algorithms. Further analysis of order parameters calculated with SPOONE unweighted, SPOONE weighted, and SPOONE weighted with a cutoff is still needed to evaluate the utility of the SPOONE algorithm.

5.4.6 Effects of Ray Density

The ray density parameter ρ_{ray} defines the number of rays per unit area shot from one particle to another to determine neighbors and neighbor weights. Choosing a ray density too small may cause the neighbor definition to be inaccurate, whereas too large a ray density may slow performance. We therefore use this section to discuss the optimal value for ray density that provides sufficiently accurate results yet does not slow performance more than necessary.

We begin by placing three square prisms along a line at random orientations (Fig. 5.2d) and observe how the SPOONE weights change as we change both the ray density and the insphere radius of the prisms R_{in}. We plot the neighbor weight between the two outer particles as a function of the area of the prism's incircle times the ray density (Fig. 5.2e). This parameter, $N_{rays} \sim \pi R_{in}^2 \rho_{ray}$, provides an order of magnitude calculation for the number of rays shot between two neighbors to determine their neighbor weight. As shown in Fig. 5.2f, the neighbor weight differs from the limiting value ($\rho_{ray} = \infty$) by a value that is bounded by $1/\sqrt{N_{rays}}$, consistent with the central limit theorem of statistics. We therefore recommend the value of ray density be chosen consistent with the user's tolerable error in weights given the particle size and shape.

5.5 Conclusions

In this chapter, we have demonstrated developments in software tools used for the advancement of solutions to problems in the field of nanoparticle self-assembly. We demonstrated a set of plugins for the HOOMD-blue simulation toolkit that with a few minor tweaks, will enable alchemical simulations in larger extended ensembles for the purpose of inverse design. We wrote a software package implementing both scaling theory calculation of effective shapes and calculations of their lattice energies. Used in succession, these calculations constitute an end-to-end prediction workflow for high-throughput screening for materials design. Lastly, we implemented the SPOONE neighbor-finding algorithm, which may give more intuitive results for systems of shaped particles, although more investigation is needed to fully evaluate its utility. All three of these tools help address significant problems in computational nanoparticle self-assembly.

CHAPTER VI

Conclusions and Outlook

In this dissertation I have presented work advancing our understanding of the interaction between the nanoparticle design handles of particle shape and polymer behavior. I have done so via computational modeling of various nanoparticle systems and development of computational methods to aid in the design process.

6.1 Summary

In Chapter II, we showed good agreement between simulation and scaling theory for non-attractive polymers grafted to anisotropic nanoparticles, demonstrating the validity of theoretical assumptions about polymer chain length relative to core size and the different chain scaling regimes within the NP polymer brush. We also observed reasonably good agreement between the effective shapes in simulation and scaling theory, only finding disagreement for elongated shapes and certain shapes in the high grafting density regime. Qualitatively, the trends in classes of effective shapes are consistent between theory and simulation throughout the phase space studied. At a high level, the different effective shapes provide those who design materials with a handle not only on the particle shape, but on the *concavity* of the effective particle shape.

In Chapter III, we worked with the Chen group to better understand their "atomic

stencil" method of controlling patch positions on shaped NPs. We provided them with a conceptual understanding and a theoretical framework to aid in understanding the physics underlying both the iodine and polymer patch behavior of their systems. This work is particularly important because their method will open new avenues for control of patch size and location on iodine coated nanoparticles. Once the individual patchy particles were understood, we abstracted our simulation model and demonstrated their assembly into open BCC and BCC-like structures, consistent with experiment. The iodine's preference for the NP (111) facets prevented patch formation in those locations, allowing the van der Waals attraction between the the gold cores to drive the system's assembly behavior.

In Chapter IV, we extended the work of Chapter III by incorporating more experimental handles into our computational models. We chose to use the truncated tetrahedron shape, which exhibits more complex faceting than many previous shapes, and we found a wider variety of patch morphologies that could be tuned to a greater degree via choice of a wider variety of experimental variables.

In Chapter V, we presented work on computational methods to solve problems in the field of NP self-assembly. We enabled new methods for computation-driven design via both high-throughput screening and inverse design with digital alchemy. We started by expanding the design space available to treat problems with digital alchemy by writing a set of plugins to the HOOMD-blue simulation toolkit. We then refined the scaling theory used in previous projects and combined it with a lattice perturbation theory to enable end-to-end prediction of the lowest energy crystal structures among a set of candidates. Finally, we presented SPOONE: a neighbor finding algorithm with the potential to define more physically intuitive particle neighborhoods for systems of anisotropic particles.

6.2 Outlook

Chapter II demonstrated that effective shapes are often concave and can be utilized to synthesize new binary lock and key nanoparticle structures. However, the assembly behavior of concave shapes has not been systematically studied like convex shapes. A deeper understanding of concave shape assembly behavior is needed before the effective shapes can be leveraged for designing new single component assemblies.

Chapters III and IV introduced an entirely new method for controlling the patch location on anisotropic particles, proposed by our collaborators and investigated by modeling and simulation. Future work will be dedicated to refining these methods towards total control of core surface masking by the masking ion. To this end, there are a few potential research questions that immediately come to mind:

1. **Can a different polymer anchoring molecule be used to alter surface masking behavior?** In Chapter III, the DFT calculations show the facet preference of the iodine may depend on the relative binding affinity of the iodine and the 2-NAT anchoring the polymer chain. Utilizing a different polymer anchor may change the preference for facet attachment, even whilst using the same masking ion.

2. **Can we use different experimental procedures to alter the surface masking?** The attachment of the iodine to the core surface is done before any polymer chains are added to the solution. During this preliminary stage, there may be some experimental handle (like temperature, etc.) that can alter the iodine's surface masking to the nanoparticle core.

Additionally, the driver of the assembly process in Chapter III is not the polymer interaction, but rather the short-range van der Waals attractions between the iodine-

poisoned pathces on the NP facets. This is not a novel assembly mechanism per se, as van der Waals attractions can often be used to induce face-face bonding in NP assemblies. What is novel, however, is the use of repulsive polymer interactions to screen out van der Waals attractions, leaving only the iodine-poisoned areas of the NP surface to interact with other NPs. As we work to gain more fine-grained control over the iodine surface masking, it is worth thinking about which iodine patterns might result in the desired crystal structures.

In Chapter V, we showed potential solutions to a few different computational problems in our field. Future work on the problem of inverse design will be primarily related to solving the complex optimization problem involved. Finding a free energy minimum in extended ensembles is hard, and its particularly hard when we open the extended ensemble to an increasing number of alchemical variables. This will require new and more inventive approaches to optimization. Additionally, future work will be needed to more thoroughly investigate the utility of the SPOONE neighbor finding algorithm. Both weighted and unweighted versions of SPOONE, along with order parameters computed with the SPOONE neighbor definitions will need further investigation across a variety of systems and particle shapes to fully evaluate SPOONE's utility.

BIBLIOGRAPHY

BIBLIOGRAPHY

[1] I. Hammami, N. M. Alabdallah, A. A. jomaa, and M. kamoun, "Gold nanoparticles: Synthesis properties and applications," *Journal of King Saud University - Science*, vol. 33, p. 101560, Oct. 2021.

[2] A. Regmi, Y. Basnet, S. Bhattarai, and S. K. Gautam, "Cadmium Sulfide Nanoparticles: Synthesis, Characterization, and Antimicrobial Study," *Journal of Nanomaterials*, vol. 2023, p. 8187000, June 2023. Publisher: Hindawi.

[3] A. Ghasempour, H. Dehghan, M. Ataee, B. Chen, Z. Zhao, M. Sedighi, X. Guo, and M.-A. Shahbazi, "Cadmium Sulfide Nanoparticles: Preparation, Characterization, and Biomedical Applications," *Molecules*, vol. 28, no. 9, 2023.

[4] X.-F. Zhang, Z.-G. Liu, W. Shen, and S. Gurunathan, "Silver Nanoparticles: Synthesis, Characterization, Properties, Applications, and Therapeutic Approaches," *International Journal of Molecular Sciences*, vol. 17, no. 9, 2016.

[5] M. Jeyaraj, S. Gurunathan, M. Qasim, M.-H. Kang, and J.-H. Kim, "A Comprehensive Review on the Synthesis, Characterization, and Biomedical Application of Platinum Nanoparticles," *Nanomaterials*, vol. 9, no. 12, 2019.

[6] W. Lohcharoenkal, L. Wang, Y. C. Chen, and Y. Rojanasakul, "Protein Nanoparticles as Drug Delivery Carriers for Cancer Therapy," vol. 2014, p. 180549, Mar. 2014. Publisher: Hindawi Publishing Corporation.

[7] J. K. Pokorski and N. F. Steinmetz, "The Art of Engineering Viral Nanoparticles," *Molecular Pharmaceutics*, vol. 8, pp. 29–43, Feb. 2011. Publisher: American Chemical Society.

[8] Z. L. Tyrrell, Y. Shen, and M. Radosz, "Fabrication of micellar nanoparticles for drug delivery through the self-assembly of block copolymers," *Topical Issue on Biomaterials*, vol. 35, pp. 1128–1143, Sept. 2010.

[9] X. Hou, T. Zaks, R. Langer, and Y. Dong, "Lipid nanoparticles for mRNA delivery," *Nature Reviews Materials*, vol. 6, pp. 1078–1094, Dec. 2021.

[10] S. Verma, S. Singh, N. Syan, P. Mathur, and V. Valecha, "Nanoparticle vesicular systems: A versatile tool for drug delivery," *J. Chem. Pharm. Res.*, vol. 2, pp. 496–509, Jan. 2010.

[11] C. Burda, X. Chen, R. Narayanan, and M. A. El-Sayed, "Chemistry and Properties of Nanocrystals of Different Shapes," *Chemical Reviews*, vol. 105, pp. 1025–1102, Apr. 2005. Publisher: American Chemical Society.

[12] A. P. Alivisatos, "Perspectives on the Physical Chemistry of Semiconductor Nanocrystals," *The Journal of Physical Chemistry*, vol. 100, pp. 13226–13239, Jan. 1996. Publisher: American Chemical Society.

[13] A. Henglein, "Small-particle research: physicochemical properties of extremely small colloidal metal and semiconductor particles," *Chemical Reviews*, vol. 89, pp. 1861–1873, Dec. 1989. Publisher: American Chemical Society.

[14] K. Kalyanasundaram, E. Borgarello, D. Duonghong, and M. Grätzel, "Cleavage of Water by Visible-Light Irradiation of Colloidal CdS Solutions; Inhibition of Photocorrosion by RuO2," *Angewandte Chemie International Edition in English*, vol. 20, pp. 987–988, Nov. 1981. Publisher: John Wiley & Sons, Ltd.

[15] A. Henglein, "Photo-Degradation and Fluorescence of Colloidal-Cadmium Sulfide in Aqueous Solution," *Berichte der Bunsengesellschaft für physikalische Chemie*, vol. 86, pp. 301–305, Apr. 1982. Publisher: John Wiley & Sons, Ltd.

[16] M. Liu, Y. Ma, H. Wu, and R. Y. Wang, "Metal Matrix–Metal Nanoparticle Composites with Tunable Melting Temperature and High Thermal Conductivity for Phase-Change Thermal Storage," *ACS Nano*, vol. 9, pp. 1341–1351, Feb. 2015. Publisher: American Chemical Society.

[17] D. Guo, G. Xie, and J. Luo, "Mechanical properties of nanoparticles: basics and applications," *Journal of Physics D: Applied Physics*, vol. 47, p. 013001, Dec. 2013. Publisher: IOP Publishing.

[18] O. Salata, "Applications of nanoparticles in biology and medicine," *Journal of Nanobiotechnology*, vol. 2, p. 3, Apr. 2004.

[19] G. Gorrasi and A. Sorrentino, "Mechanical milling as a technology to produce structural and functional bio-nanocomposites," *Green Chem.*, vol. 17, no. 5, pp. 2610–2625, 2015. Publisher: The Royal Society of Chemistry.

[20] A.-G. Niculescu, D. E. Mihaiescu, and A. M. Grumezescu, "A Review of Microfluidic Experimental Designs for Nanoparticle Synthesis," *International Journal of Molecular Sciences*, vol. 23, no. 15, 2022.

[21] J. P. Rolland, E. C. Hagberg, G. M. Denison, K. R. Carter, and J. M. De Simone, "High-Resolution Soft Lithography: Enabling Materials for Nanotechnologies," *Angewandte Chemie International Edition*, vol. 43, pp. 5796–5799, Nov. 2004. Publisher: John Wiley & Sons, Ltd.

[22] P. Machac, S. Cichon, L. Lapcak, and L. Fekete, "Graphene prepared by chemical vapour deposition process," *Graphene Technology*, vol. 5, pp. 9–17, June 2020.

[23] S. Das and V. Srivastava, "Synthesis and Characterization of ZnO–MgO Nanocomposite by Co-precipitation Method," *Smart Science*, vol. 4, pp. 1–6, Dec. 2016.

[24] G. Riess, "Micellization of block copolymers," *Progress in Polymer Science*, vol. 28, pp. 1107–1170, July 2003.

[25] T. Imura, H. Yanagishita, J. Ohira, H. Sakai, M. Abe, and D. Kitamoto, "Thermodynamically stable vesicle formation from glycolipid biosurfactant sponge phase," *Colloids and Surfaces B: Biointerfaces*, vol. 43, pp. 115–121, June 2005.

[26] C. J. Hawker and J. M. J. Frechet, "Preparation of polymers with controlled molecular architecture. A new convergent approach to dendritic macromolecules," *Journal of the American Chemical Society*, vol. 112, pp. 7638–7647, Oct. 1990. Publisher: American Chemical Society.

[27] T. K. Sau and C. J. Murphy, "Self-Assembly Patterns Formed upon Solvent Evaporation of Aqueous Cetyltrimethylammonium Bromide-Coated Gold Nanoparticles of Various Shapes," *Langmuir*, vol. 21, pp. 2923–2929, Mar. 2005. Publisher: American Chemical Society.

[28] R. Deshmukh, P. Wagh, and J. Naik, "Solvent evaporation and spray drying technique for micro- and nanospheres/particles preparation: A review," *Drying Technology*, vol. 34, pp. 1758–1772, Nov. 2016. Publisher: Taylor & Francis.

[29] A. Böker, J. He, T. Emrick, and T. P. Russell, "Self-assembly of nanoparticles at interfaces," *Soft Matter*, vol. 3, no. 10, pp. 1231–1248, 2007. Publisher: The Royal Society of Chemistry.

[30] S. A. Davis, M. Breulmann, K. H. Rhodes, B. Zhang, and S. Mann, "Template-Directed Assembly Using Nanoparticle Building blocks: A Nanotectonic Approach to Organized Materials," *Chemistry of Materials*, vol. 13, pp. 3218–3226, Oct. 2001. Publisher: American Chemical Society.

[31] T. Ding, K. Song, K. Clays, and C.-H. Tung, "Fabrication of 3D Photonic Crystals of Ellipsoids: Convective Self-Assembly in Magnetic Field," *Advanced Materials*, vol. 21, pp. 1936–1940, May 2009. Publisher: John Wiley & Sons, Ltd.

[32] M. Mittal and E. M. Furst, "Electric Field-Directed Convective Assembly of Ellipsoidal Colloidal Particles to Create Optically and Mechanically Anisotropic Thin Films," *Advanced Functional Materials*, vol. 19, pp. 3271–3278, Oct. 2009. Publisher: John Wiley & Sons, Ltd.

[33] C. A. Mirkin, R. L. Letsinger, R. C. Mucic, and J. J. Storhoff, "A dna-based method for rationally assmebling nanoparticles into macroscopic materials," *Nature*, vol. 382, no. 6592, pp. 607–609, 1996.

[34] A. P. Alivisatos, K. P. Johnsson, X. Peng, T. E. Wilson, C. J. Loweth, M. P. Bruchez, and P. G. Schultz, "Organization of 'nanocrystal molecules' using DNA," *Nature*, vol. 382, pp. 609–611, Aug. 1996.

[35] S. Sacanna, M. Korpics, K. Rodriguez, L. Colon-Melendez, S. Kim, D. J. Pine, and G. Yi, "Shaping colloids for self-assembly," *Nat. Commun*, vol. 4, p. 1688, 2013.

[36] P. F. Damasceno, M. Engel, and S. C. Glotzer, "Predictive self-assembly of polyhedra into complex structures," *Science*, vol. 337, no. 6093, pp. 453–457, 2012.

[37] P. F. Damasceno, M. Engel, and S. C. Glotzer, "Crystalline assemblies and densest packings of a family of truncated tetrahedra and the role of directional entropic forces," *ACS Nano*, vol. 6, no. 1, pp. 609–614, 2011.

[38] Y. Lim, S. Lee, and S. C. Glotzer, "Engineering the Thermodynamic Stability and Metastability of Mesophases of Colloidal Bipyramids through Shape Entropy," *ACS Nano*, vol. 17, pp. 4287–4295, Mar. 2023. Publisher: American Chemical Society.

[39] S. Lee, T. Vo, and S. C. Glotzer, "Entropy compartmentalization stabilizes open host–guest colloidal clathrates," *Nature Chemistry*, vol. 15, pp. 905–912, July 2023.

[40] T. Dwyer, T. C. Moore, J. A. Anderson, and S. C. Glotzer, "Tunable assembly of host–guest colloidal crystals," *Soft Matter*, vol. 19, no. 36, pp. 7011–7019, 2023. Publisher: The Royal Society of Chemistry.

[41] S. Lee and S. C. Glotzer, "Entropically engineered formation of fivefold and icosahedral twinned clusters of colloidal shapes," *Nature Communications*, vol. 13, p. 7362, Nov. 2022.

[42] Y. Zhou, R. K. Cersonsky, and S. C. Glotzer, "A route to hierarchical assembly of colloidal diamond," *Soft Matter*, vol. 18, no. 2, pp. 304–311, 2022. Publisher: The Royal Society of Chemistry.

[43] K. Je, S. Lee, E. G. Teich, M. Engel, and S. C. Glotzer, "Entropic formation of a thermodynamically stable colloidal quasicrystal with negligible phason strain," *Proceedings of the National Academy of Sciences*, vol. 118, p. e2011799118, Feb. 2021. Publisher: Proceedings of the National Academy of Sciences.

[44] T. C. Moore, J. A. Anderson, and S. C. Glotzer, "Shape-driven entropic self-assembly of an open, reconfigurable, binary host–guest colloidal crystal," *Soft Matter*, vol. 17, pp. 2840–2848, 2021.

[45] Y. Geng, G. v. Anders, P. M. Dodd, J. Dshemuchadse, and S. C. Glotzer, "Engineering entropy for the inverse design of colloidal crystals from hard shapes," *Science Advances*, vol. 5, no. 7, p. eaaw0514, 2019. _eprint: https://www.science.org/doi/pdf/10.1126/sciadv.aaw0514.

[46] S. Lee, E. G. Teich, M. Engel, and S. C. Glotzer, "Entropic colloidal crystallization pathways via fluid-fluid transitions and multidimensional prenucleation motifs," *P. Natl. Acad. Sci. USA*, vol. 116, pp. 14843–14851, 2019.

[47] A. S. Karas, J. Dshemuchadse, G. van Anders, and S. C. Glotzer, "Phase behavior and design rules for plastic colloidal crystals of hard polyhedra via consideration of directional entropic forces," *Soft Matter*, vol. 15, no. 27, pp. 5380–5389, 2019. Publisher: The Royal Society of Chemistry.

[48] J. Gong, R. S. Newman, M. Engel, M. Zhao, F. Bian, S. C. Glotzer, and Z. Tang, "Shape-dependent ordering of gold nanocrystals into large-scale superlattices," *Nature Communications*, vol. 8, p. 14038, Jan. 2017.

[49] P. F. Damasceno, A. S. Karas, B. A. Schultz, M. Engel, and S. C. Glotzer, "Controlling Chirality of Entropic Crystals," *Phys. Rev. Lett.*, vol. 115, p. 158303, Oct. 2015. Publisher: American Physical Society.

[50] Jin Rongchao, Cao YunWei, Mirkin Chad A., Kelly K. L., Schatz George C., and Zheng J. G., "Photoinduced Conversion of Silver Nanospheres to Nanoprisms," *Science*, vol. 294, pp. 1901–1903, Nov. 2001. Publisher: American Association for the Advancement of Science.

[51] S. Xu, Z. Nie, M. Seo, P. Lewis, E. Kumacheva, H. A. Stone, P. Garstecki, D. B. Weibel, I. Gitlin, and G. M. Whitesides, "Generation of Monodisperse Particles by Using Microfluidics: Control over Size, Shape, and Composition," *Angewandte Chemie International Edition*, vol. 44, pp. 724–728, Jan. 2005. Publisher: John Wiley & Sons, Ltd.

[52] M. A. Boles, M. Engel, and D. V. Talapin, "Self-assembly of colloidal nanocrystals: From intricate structures to functional materials," *Chem Rev*, vol. 116, pp. 11220–11289, 2016.

[53] S. C. Glotzer and M. Solomon, "Anisotropy of building blocks and their assembly into complex structures," *Nat. Mater.*, vol. 6, no. 8, pp. 557–562, 2007.

[54] J. S. Kahn and O. Gang, "Designer nanomaterials through programmable assembly," *Angewandte Chemie International Edition*, vol. 61, no. 3, 2021.

[55] G. van Anders, N. K. Ahmed, R. Smith, M. Engel, and S. C. Glotzer, "Entropically patchy partcles: Engineering valence through shape entropy," *ACS Nano*, vol. 8, no. 1, pp. 931–940, 2014.

[56] T. Vo and S. C. Glotzer, "A theory of entropic bonding," *P. Natl. Acad. Sci. USA*, vol. 119, no. 4, p. e2116414119, 2022.

[57] M. R. Jones, R. J. Macfarlane, B. Lee, J. Zhang, K. L. Young, A. J. Senesi, and C. A. Mirkin, "DNA-nanoparticle superlattices formed from anisotropic building blocks," *Nature Materials*, vol. 9, pp. 913–917, Nov. 2010.

[58] J. Henzie, M. Grunwald, A. Widmer-Cooper, P. L. Geissler, and P. Yang, "Mesophase behaviour of polyhedral particles," *Nat. Mater.*, vol. 11, pp. 131–137, 2012.

[59] H. Lin, S. Lee, L. Sun, M. Spellings, M. Engel, S. C. Glotzer, and C. A. Mirkin, "Clathrate colloidal crystals," *Science*, vol. 355, pp. 931–935, Mar. 2017. Publisher: American Association for the Advancement of Science.

[60] M. N. O'Brien, M. R. Jones, B. Lee, and C. A. Mirkin, "Anisotropic nanoparticle complementarity in dna-mediated co-crystallization," *Nat. Mater.*, vol. 14, pp. 833–839, 2015.

[61] F. Lu, T. Vo, Y. Zhang, A. Frenkel, K. G. Yager, S. Kumar, and O. Gang, "Unusual packing of soft-shelled nanocubes," *Science Advances*, vol. 5, p. eaaw2399, May 2019.

[62] W. Liu, M. Tagawa, H. I. Xin, T. Wang, H. Emamy, H. Li, K. Yager, F. W. Starr, A. V. Tkachenko, and O. Gang, "Diamond family of nanoparticle superlattices," *Science*, vol. 351, pp. 582–586, 2016.

[63] X. Ye, J. Chen, M. Engel, J. A. Millan, W. Li, L. Qi, G. Xing, J. E. Collins, C. R. Kagan, J. Li, S. C. Glotzer, and C. B. Murray, "Competition of shape and interaction patchiness for self-assembling nanoplates," *Nat. Chem*, vol. 5, pp. 466–473, 2013.

[64] K. C. Elbert, W. Zygmunt, T. Vo, C. M. Vera, D. J. Rosen, N. M. Krook, S. C. Glotzer, and C. B. Murray, "Anisotropic nanocrystal shape and ligand design for co-assembly through inverse design," *Nat. Chem*, Submitted.

[65] P. F. Damasceno, M. Engel, and S. C. Glotzer, "Predictive Self-Assembly of Polyhedra into Complex Structures," *Science*, vol. 337, pp. 453–457, July 2012. Publisher: American Association for the Advancement of Science.

[66] U. Agarwal and F. A. Escobeda, "Mesophase behaviour of polyhedral particles," *Nat. Mater.*, vol. 10, pp. 230–235, 2011.

[67] A. Gantapara, J. De Graaf, R. Van Roij, and M. Dijkstra, "Phase diagram and structural diversity of a family of truncated cubes: Degenerate close-packed structures and vacancy-rich states," *Phys. Rev. Lett.*, vol. 11, no. 1, p. 015501, 2013.

[68] P. F. Damasceno, M. Engel, and S. C. Glotzer, "Crystalline Assemblies and Densest Packings of a Family of Truncated Tetrahedra and the Role of Directional Entropic Forces," *ACS Nano*, vol. 6, pp. 609–614, Jan. 2012. Publisher: American Chemical Society.

[69] C. R. Laramy, M. N. O'Brien, and C. A. Mirkin, "Crystal engineering with dna," *Nat. Rev. Mat*, vol. 4, pp. 201–224, 2019.

[70] T. Paik, T. R. Gordon, A. M. Prantner, H. Yun, and C. B. Murray, "Designing tripodal and triangular gadolinium oxide nanoplates and self-assembled nanofibrils as potential multimodal bioimaging probes," *ACS Nano*, vol. 7, no. 3, pp. 2850–2859, 2013.

[71] Y. Liu, K. Deng, J. Yang, X. Wu, X. Fan, M. Tang, and Z. Quan, "Shape-directed self-assembly of nanodumbbells into superstructure polymorphs," *Chem. Sci*, vol. 11, p. 4065, 2020.

[72] E. V. Shevchenko, D. V. Talapin, N. A. Kotov, S. O'Brien, and C. B. Murray, "Structural diversity in binary nanoparticle superlattices," *Nature*, vol. 439, pp. 55–59, 2006.

[73] S. K. Kumar, B. C. Benicewicz, R. A. Vaia, and K. I. Winey, "50th anniversary perspective: Are polymer nanocomposites practical for applications?," *Macromolecules*, vol. 50, no. 3, pp. 714–731, 2017.

[74] W. Chen, R. Cordero, H. Tran, and C. K. Ober, "50th anniversary perspective: Polymer brushes: Novel surfaces for future materials," *Macromolecules*, vol. 50, no. 3, pp. 4089–4113, 2017.

[75] K. C. Elbert, W. Zygmunt, T. Vo, C. M. Vara, D. J. Rosen, N. M. Krook, S. C. Glotzer, and C. B. Murray, "Anisotropic nanocrystal shape and ligand design for co-assembly," *Science Advances*, vol. 7, p. eabf9402, June 2021.

[76] T. Paik, D. K. Ko, T. R. Gordon, V. Doan-Nguyen, and C. B. Murray, "Studies of liquid crystalline self-assembly of gdf3 nanoplates by in-plane, out-of-plane saxs," *ACS Nano*, vol. 5, no. 10, pp. 8322–8330, 2011.

[77] A. Santos, J. A. Millan, and S. C. Glotzer, "Facetted patchy particles through entropy-driven patterning of mixed ligand sams," *Nanoscale*, vol. 4, pp. 2640–2650, 2012.

[78] C. Singh, P. K. Ghorai, M. A. Horsch, A. M. Jackson, R. G. Larson, F. Stellacci, and S. C. Glotzer, "Entropy-mediated patterning of surfactant-coated nanoparticles and surfaces," *Phys. Rev. Lett.*, vol. 99, p. 226106, Nov 2007.

[79] J. A. Anderson, J. Glaser, and S. C. Glotzer, "HOOMD-blue: A Python package for high-performance molecular dynamics and hard particle Monte Carlo simulations," *Computational Materials Science*, vol. 173, p. 109363, Feb. 2020.

[80] V. Ramasubramani, B. D. Dice, E. S. Harper, M. P. Spellings, J. A. Anderson, and S. C. Glotzer, "freud: A software suite for high throughput analysis of particle simulation data," *Computer Physics Communications*, vol. 254, p. 107275, Sept. 2020.

[81] C. S. Adorf, P. M. Dodd, V. Ramasubramani, and S. C. Glotzer, "Simple data and workflow management with the signac framework," *Computational Materials Science*, vol. 146, pp. 220–229, Apr. 2018.

[82] T. Waltmann and T. Vo, "The *agrippa* python package," 2023. Available at `https://github.com/glotzerlab/agrippa`.

[83] V. Ramasubramani, T. Vo, J. A. Anderson, and S. C. Glotzer, "A mean-field approach to simulating anisotropic particles," *The Journal of Chemical Physics*, vol. 153, p. 084106, Aug. 2020. Publisher: American Institute of Physics.

[84] K. Krmer and G. S. Grest, "Dynamics of entangled linear polymer melts: A molecular-dynamics simulation," *J. Chem. Phys.*, vol. 94, pp. 5057–5086, 1990.

[85] M. Rubinstein and R. Colby, *Polymer Physics*. Oxford University Press, 2003.

[86] F. Lu, T. Vo, Y. Zhang, A. Frenkel, K. G. Yager, S. Kumar, and O. Gang, "Unusual packing of soft-shelled nanocubes," *Science Advances*, vol. 5, no. 5, pp. 1–9, 2019.

[87] R. A. LaCour, T. C. Moore, and S. C. Glotzer, "Tuning Stoichiometry to Promote Formation of Binary Colloidal Superlattices," *Physical Review Letters*, vol. 128, p. 188001, May 2022. Publisher: American Physical Society.

[88] F. Smallenburg, L. Filion, M. Marechal, and M. Dijkstra, "Vacancy-stabilized crystalline order in hard cubes," *P. Natl. Acad. Sci. USA*, vol. 109, no. 44, pp. 17886–17890, 2012.

[89] U. K. Cheang and M. J. Kim, "Self-assembly of robotic micro- and nanoswimmers using magnetic nanoparticles," *Journal of Nanoparticle Research*, vol. 17, p. 145, Mar. 2015.

[90] R. Singh and J. W. Lillard, "Nanoparticle-based targeted drug delivery," *Special Issue: Structural Biology*, vol. 86, pp. 215–223, June 2009.

[91] J. Dintinger, S. Mühlig, C. Rockstuhl, and T. Scharf, "A bottom-up approach to fabricate optical metamaterials by self-assembled metallic nanoparticles," *Opt. Mater. Express*, vol. 2, pp. 269–278, Mar. 2012. Publisher: Optica Publishing Group.

[92] J. Bauer, L. R. Meza, T. A. Schaedler, R. Schwaiger, X. Zheng, and L. Valdevit, "Nanolattices: An Emerging Class of Mechanical Metamaterials," *Advanced Materials*, vol. 29, p. 1701850, Oct. 2017. Publisher: John Wiley & Sons, Ltd.

[93] M. J. Kim, M. A. Cruz, Z. Chen, H. Xu, M. Brown, K. A. Fichthorn, and B. J. Wiley, "Isotropic Iodide Adsorption Causes Anisotropic Growth of Copper Microplates," *Chemistry of Materials*, vol. 33, pp. 881–891, Feb. 2021. Publisher: American Chemical Society.

[94] M. J. Kim, S. Alvarez, Z. Chen, K. A. Fichthorn, and B. J. Wiley, "Single-Crystal Electrochemistry Reveals Why Metal Nanowires Grow," *Journal of the American Chemical Society*, vol. 140, pp. 14740–14746, Nov. 2018. Publisher: American Chemical Society.

[95] J. Kim and K. A. Fichthorn, "The influence of iodide on the solution-phase growth of Cu microplates: a multi-scale theoretical analysis from first principles," *Faraday Discuss.*, vol. 235, no. 0, pp. 273–288, 2022. Publisher: The Royal Society of Chemistry.

[96] A. Kim, T. Vo, H. An, P. Banerjee, L. Yao, S. Zhou, C. Kim, D. J. Milliron, S. C. Glotzer, and Q. Chen, "Symmetry-breaking in patch formation on triangular gold nanoparticles by asymmetric polymer grafting," *Nature Communications*, vol. 13, p. 6774, Nov. 2022.

[97] P. J. Steinhardt, D. R. Nelson, and M. Ronchetti, "Bond-orientational order in liquids and glasses," *Phys. Rev. B*, vol. 28, pp. 784–805, July 1983. Publisher: American Physical Society.

[98] J. S. Gardner, M. J. P. Gingras, and J. E. Greedan, "Magnetic pyrochlore oxides," *Rev. Mod. Phys.*, vol. 82, pp. 53–107, Jan 2010.

[99] A. Haji-Akbari, M. Engel, A. S. Keys, X. Zheng, R. G. Petschek, P. Palffy-Muhoray, and S. C. Glotzer, "Disordered, quasicrystalline and crystalline phases of densely packed tetrahedra," *Nature*, vol. 462, pp. 773–777, 2009.

[100] Z. Cheng and M. R. Jones, "Assembly of planar chiral superlattices from achiral building blocks," *Nature Communications*, vol. 13, p. 4207, July 2022.

[101] S. Zhou, J. Li, J. Lu, H. Liu, J.-Y. Kim, A. Kim, L. Yao, C. Liu, C. Qian, Z. D. Hood, X. Lin, W. Chen, T. E. Gage, I. Arslan, A. Travesset, K. Sun, N. A. Kotov, and Q. Chen, "Chiral assemblies of pinwheel superlattices on substrates," *Nature*, vol. 612, pp. 259–265, Dec. 2022.

[102] A. Haji-Akbari, M. Engel, and S. C. Glotzer, "Phase diagram of hard tetrahedra," *J. Chem. Phys*, vol. 135, p. 194101, 2011.

[103] A. B. Pawar and I. Kretzschmar, "Fabrication, Assembly, and Application of Patchy Particles," *Macromolecular Rapid Communications*, vol. 31, pp. 150–168, Jan. 2010. Publisher: John Wiley & Sons, Ltd.

[104] S. M. Ng, M. Koneswaran, and R. Narayanaswamy, "A review on fluorescent inorganic nanoparticles for optical sensing applications," *RSC Adv.*, vol. 6, no. 26, pp. 21624–21661, 2016. Publisher: The Royal Society of Chemistry.

[105] M. B. Gawande, A. Goswami, T. Asefa, H. Guo, A. V. Biradar, D.-L. Peng, R. Zboril, and R. S. Varma, "Core–shell nanoparticles: synthesis and applications in catalysis and electrocatalysis," *Chem. Soc. Rev.*, vol. 44, no. 21, pp. 7540–7590, 2015. Publisher: The Royal Society of Chemistry.

[106] K. McNamara and S. A. M. Tofail, "Nanoparticles in biomedical applications," *Advances in Physics: X*, vol. 2, pp. 54–88, Jan. 2017. Publisher: Taylor & Francis.

[107] A. H. Gröschel, A. Walther, T. I. Löbling, F. H. Schacher, H. Schmalz, and A. H. E. Müller, "Guided hierarchical co-assembly of soft patchy nanoparticles," *Nature*, vol. 503, pp. 247–251, Nov. 2013.

[108] Q. Ong, Z. Luo, and F. Stellacci, "Characterization of Ligand Shell for Mixed-Ligand Coated Gold Nanoparticles," *Accounts of Chemical Research*, vol. 50, pp. 1911–1919, Aug. 2017. Publisher: American Chemical Society.

[109] J. A. Anderson, C. D. Lorenz, and A. Travesset, "General purpose molecular dynamics simulations fully implemented on graphics processing units," *J. Comp. Phys*, vol. 227, pp. 5342–5359, 2008.

[110] J. Glaser, T. D. Nguyen, J. A. Anderson, P. Liu, F. Spiga, J. A. Millan, D. C. Morse, and S. C. Glotzer, "Strong scaling of general-purpose molecular dynamics simulations on gpus," *Comp. Phys. Comm*, vol. 192, pp. 97–107, 2015.

[111] J. A. Anderson, M. E. Irrgang, and S. C. Glotzer, "Scalable metropolis monte carlo for simulation of hard shapes," *Comp. Phys. Comm*, vol. 204, pp. 21–30, 2016.

[112] G. van Anders, D. Klotsa, A. S. Karas, P. M. Dodd, and S. C. Glotzer, "Digital Alchemy for Materials Design: Colloids and Beyond," *ACS Nano*, vol. 9, pp. 9542–9553, Oct. 2015. Publisher: American Chemical Society.

[113] L. Y. Rivera-Rivera, T. C. Moore, and S. C. Glotzer, "Inverse design of triblock Janus spheres for self-assembly of complex structures in the crystallization slot via digital alchemy," *Soft Matter*, vol. 19, no. 15, pp. 2726–2736, 2023. Publisher: The Royal Society of Chemistry.

[114] F. J. Vesely, "Angular Monte Carlo integration using quaternion parameters: a spherical reference potential for CCl4," *Journal of Computational Physics*, vol. 47, no. 2, pp. 291–296, 1982.

[115] K. C. Elbert, T. Vo, N. M. Krook, W. Zygmunt, P. Jungmi, K. G. Yager, R. J. Composto, S. C. Glotzer, and C. B. Murray, "Dendrimer Ligand Directed Nanoplate Assembly," *ACS Nano*, vol. 13, pp. 14241–14251, 2019.

[116] Y. Tian, J. R. Lhermitte, L. Bai, T. Vo, H. L. Xin, H. Li, R. Li, M. Fukuto, K. G. Yager, J. S. Kahn, Y. Xiong, B. Minevich, S. K. Kumar, and O. Gang, "Ordered three-dimensional nanomaterials using dna-prescribed and valence-controlled material voxels," *Nat. Mater.*, 2020.

[117] C. S. Adorf, V. Ramasubramani, J. A. Anderson, and S. C. Glotzer, "How to professionally develop reusable scientific software—and when not to," *Computing in Science and Engineering*, vol. 21, no. 2, pp. 66–79, 2019.

[118] A. Haji-Akbari and S. C. Glotzer, "Strong orientational coordinates and orientational order parameters for symmetric objects," *Journal of Physics A: Mathematical and Theoretical*, vol. 48, p. 485201, Oct. 2015. Publisher: IOP Publishing.

[119] L. Filion, M. Hermes, R. Ni, and M. Dijkstra, "Crystal nucleation of hard spheres using molecular dynamics, umbrella sampling, and forward flux sampling: A comparison of simulation techniques," *The Journal of Chemical Physics*, vol. 133, p. 244115, Dec. 2010.

[120] J. A. Anderson, J. Antonaglia, J. A. Millan, M. Engel, and S. C. Glotzer, "Shape and symmetry determine two-dimensional melting transitions of hard regular polygons," *Phys. Rev. X*, vol. 7, p. 021001, 2017.

[121] E. G. Teich, G. van Anders, and S. C. Glotzer, "Identity crisis in alchemical space drives the entropic colloidal glass transition," *Nature Communications*, vol. 10, p. 64, Jan. 2019.

[122] J. Higham and R. H. Henchman, "Locally adaptive method to define coordination shell," *The Journal of Chemical Physics*, vol. 145, p. 084108, Aug. 2016. Publisher: American Institute of Physics.

[123] J. A. van Meel, L. Filion, C. Valeriani, and D. Frenkel, "A parameter-free, solid-angle based, nearest-neighbor algorithm," *The Journal of Chemical Physics*, vol. 136, p. 234107, June 2012. Publisher: American Institute of Physics.

[124] Intel, "High performance ray tracing with *embree*," 2024. Available at `https://www.embree.org/`.